PAPER

Check for updates

A bioinspired layered hydrogel actuator *via* L-ascorbic acid-triggered interfacial self-growth from a stiff hydrogel†

Rongnian Xu,* Yuxin Gao, Yingying Lai, Chengyan Zhang, Wenbo Jia and Qiangbing Wei [ID] *

Stimuli-responsive layered hydrogel actuators are highly attractive for broad applications in soft robots, intelligent devices, *etc.*, owing to their softness, asymmetric responsiveness and deformability. However, current layered hydrogel actuators suffer from serious challenges such as tedious preparation, uncontrollable layer thickness and weak interfacial bonding force. Herein, we put forward a facile and highly efficient self-growing method to prepare a layered hydrogel actuator from a stiff hydrogel substrate by crafting L-ascorbic acid (Vc)-triggered interfacial radical polymerization. The redox reaction between Vc and confined Fe^{3+} in the stiff hydrogel substrate could produce Fe^{2+} catalysts, resulting in surface catalytically initiated radical polymerization (SCIRP) at room temperature. Various layered hydrogels were prepared rapidly and the thickness of the grown hydrogel layer can be accurately controlled. The obtained layered hydrogel exhibits asymmetric structural layers consisting of a dense layer and a porous layer, as well as a strong interfacial bonding force of about 250 N m⁻¹ between the porous layer and the stiff substrate. Furthermore, a thermo-responsive layered hydrogel actuator was developed, which showed reversible underwater bending ability in response to temperature changes and can also be designed as a smart manipulator to capture objects underwater. This work provides a novel and feasible approach for the highly efficient and controllable preparation of layered hydrogel actuators, which will find promising applications in the fields of soft robots, intelligent devices, sensors and so on.

Introduction

Nature provides perpetual inspirations for the design and fabrication of versatile intelligent materials with actuating behaviors in response to external stimuli.[1–3] Similarly, stimuli-responsive hydrogels are considered as promising bionic intelligent materials due to their softness, wetness and stimuli-responsiveness[4–7] and have shown potential applications in intelligent devices,[8,9] artificial muscles,[10,11] soft robots[12–15] and sensors.[16,17] The shapes and volumes of responsive hydrogels can be reversibly changed due to phase separation induced by changes of interactions between polymer chains and water molecules. Such changes further lead to mechanical deformations, *e.g.*, bending, twisting, walking and crawling, under different external stimuli such as temperature,[18] pH,[19]

light,[20,21] salt,[22] ionic strength[23] and so on. These fantastic actuating phenomena have motivated the emergence of numerous hydrogel actuators, while the conventional hydrogels are typically homogeneous. Isotropic hydrogels usually exhibit slow and small deformation due to the limited diffusion of water molecules and simple motion patterns. Thus, much research effort has been devoted to developing hydrogel actuators with heterogeneous structures.[24]

Most of the recent significant advances have been focused on layered hydrogel actuators.[25–27] Typically, layered hydrogel actuators possess an obvious two-layer structure with asymmetric responsiveness and mechanical properties to undergo different swelling and deswelling upon external stimuli. A variety of strategies have been developed to prepare layered hydrogel actuators including chemical vapor deposition,[28] electrophoresis,[29] microfluidics,[30] step polymerization,[31,32] salt leaching[33] and so on. However, there remain several limitations that hinder the extensive applications of layered hydrogels. Typically, the bilayer structure tends to be delaminated after several repetitive actuations because of the weak interfacial bonding force. Furthermore, it has been proved that the response rate of layered hydrogels is inversely proportional to

Key Laboratory of Eco-functional Polymer Materials of the Ministry of Education, College of Chemistry and Chemical Engineering, Northwest Normal University, Lanzhou 730070, China. E-mail: weiqiangbing@nwnu.edu.cn, xurongnian@nwnu.edu.cn

the thickness of the responsive layer,[34] while the thickness of the responsive layer is difficult to accurately control by current fabrication methods. Besides, the aforementioned approaches for the preparation of layered hydrogels involve multi-step procedures, which are time-consuming and difficult for large-scale preparation. Therefore, it is still extremely challenging to develop a facile and effective method to fulfill the demand of controllable preparation of layered hydrogel actuators with a strong interfacial bonding force.

The self-growing strategy has attracted great attention for the preparation of hydrogel materials in recent years.[35–37] In our previous study, a method named UV-triggered surface catalytically initiated radical polymerization (UV-SCIRP) was proposed to prepare layered hydrogel structures by *in situ* production of Fe^{2+} ion catalysts on the Fe^{3+}-loaded hydrogel substrate *via* UV exposure.[38,39] Herein, we develop a novel self-growing method to fabricate a robust layered hydrogel actuator by crafting Vc-triggered interfacial radical polymerization from a stiff hydrogel. On brushing Vc solution on the Fe^{3+} containing poly(acrylamide-acrylic acid) stiff hydrogel substrate (PAM-PAA/Fe^{3+}), the successive redox reaction between Vc and Fe^{3+} generates an Fe^{2+} catalyst to perform surface catalytically initiated radical polymerization (SCIRP) at room temperature. The demonstrated strategy enables the rapid growth of various layered hydrogels with accurate control of the thickness of the grown layer. More importantly, the obtained layered hydrogels

exhibit a high interfacial bonding force and an asymmetric thermo-responsive feature. The thermo-responsive layered hydrogel actuator is able to reversibly bend underwater in response to different temperatures and can also be used as an underwater manipulator to grab objects. The demonstrated Vc-triggered interfacial radical polymerization enables the facile and controlled fabrication of layered hydrogel actuators *via* a novel self-growing method, which will promote the practical applications of layered hydrogels in intelligent actuators, soft robots, mechanical manipulators and so on.

Results and discussion

In nature, the humidity-induced bending of pine cones is one of the best-known examples used to design heterogeneous hydrogel actuators. The scale of a pine cone is composed of two layers with distinct structural organizations, *i.e.*, a fibrous sclerenchyma layer and a porous sclereid layer. The length of the fibrous layer remains constant, while the porous component shrinks with drying and swells with hydration, generating a local strain. Such a strain induced by changes in humidity results in the reversible deformation of the pine cone[40,41] (Fig. 1a). Inspired by the reversible deformation of pine cones, a layered hydrogel actuator with two distinct structural layers, a dense and stiff layer and a porous responsive layer, was
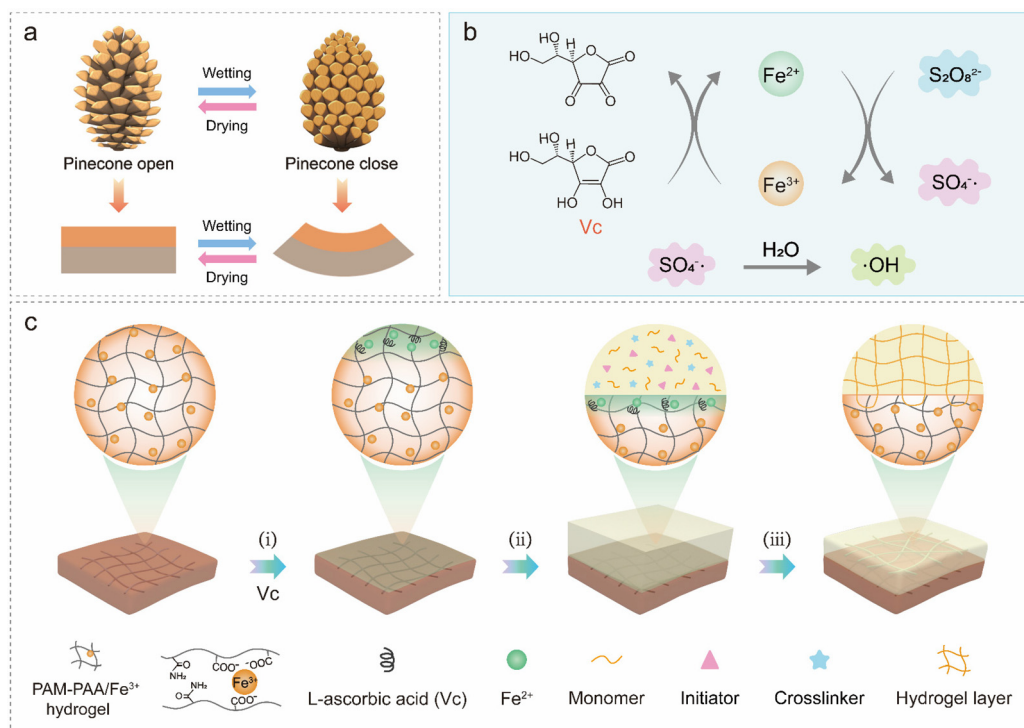

Fig. 1 (a) The schematic diagram of the closed (wet) and open (dry) states of pine cones. (b) The schematic illustration of the Vc-Fe^{3+} redox system to produce Fe^{2+} and catalytically decompose $S_2O_8^{2-}$ into $SO_4^{\cdot-}$ at room temperature. (c) The diagram of the preparation process of the layered hydrogel: (i) brushing Vc solution on the surface of the PAM-PAA/Fe^{3+} hydrogel substrate surface to produce an Fe^{2+} catalyst; (ii) immersing the PAM-PAA/Fe^{3+} hydrogel substrate after reduction with Vc in the monomer solution to perform SCIRP; (iii) a new hydrogel layer (yellow network) was grown on the top of the PAM-PAA/Fe^{3+} hydrogel substrate and the layered hydrogel was obtained.

designed and prepared using Vc-triggered interfacial radical polymerization. As shown in Fig. 1b, Vc can reduce Fe^{3+} to Fe^{2+},[42,43] which further catalytically decomposes $S_2O_8^{2-}$ into $SO_4^{\cdot-}$ radicals. The generated $SO_4^{\cdot-}$ radicals react with water to form $\cdot OH$ radicals. Similarly, the reduction of confined Fe^{3+} in the PAM-PAA/Fe^{3+} stiff hydrogel substrate by Vc could produce sufficient $SO_4^{\cdot-}$ and $\cdot OH$ radicals to trigger interfacial polymerization, resulting in rapid self-growth of a porous hydrogel layer on the substrate surface to form a layered hydrogel. The detailed preparation process is illustrated in Fig. 1c. Firstly, Vc solution with a certain concentration was brushed on the surface of PAM-PAA/Fe^{3+} hydrogel substrates to generate Fe^{2+} catalysts (Fig. 1c-i). Subsequently, the hydrogel substrate with Fe^{2+} catalysts on the surface was immersed in a monomer solution with the $S_2O_8^{2-}$ initiator and crosslinker, to perform SCIRP at the solid–liquid interface at room temperature (Fig. 1c-ii). Consequently, a fresh hydrogel layer (light yellow network) was rapidly grown on the surface of the hydrogel substrate (brown network) (Fig. 1c-iii). The prepared layered hydrogel contains the original stiff hydrogel substrate and freshly grown porous hydrogel layer and can be named the A&B

layered hydrogel (A and B represent the components of the stiff hydrogel substrate and grown hydrogel layer, respectively). Fig. S1† shows that a pentagon-like layered hydrogel (left) can be constructed and it becomes fluorescent after dyeing with 2 mg mL^{-1} rhodamine B (right).

The interfacial reduction of Fe^{3+} triggered by Vc was visually indicated by the color change of the PAM-PAA/Fe^{3+} stiff hydrogel. In Fig. 2a, the logo under the stiff hydrogel can be clearly observed through the original hydrogel, whereas it appears dusky through the hydrogel after reduction for 2 min and 6 min. The transmittance of the hydrogel substrate was further measured and it was found to gradually decrease with the increase of Vc reduction time at wavelengths ranging from 400 nm to 800 nm (Fig. 2b). It is speculated that the decrease of the transmittance of the hydrogel was probably caused by the formation of a surface porous structure arising from the reduction of Fe^{3+} to Fe^{2+}. The surface morphology of the PAM-PAA/Fe^{3+} hydrogel substrate with different reduction times was also studied by scanning electron microscopy (SEM). Compared with the dense and homogeneous structure of the original hydrogel without reduction (Fig. 2c), an obvious
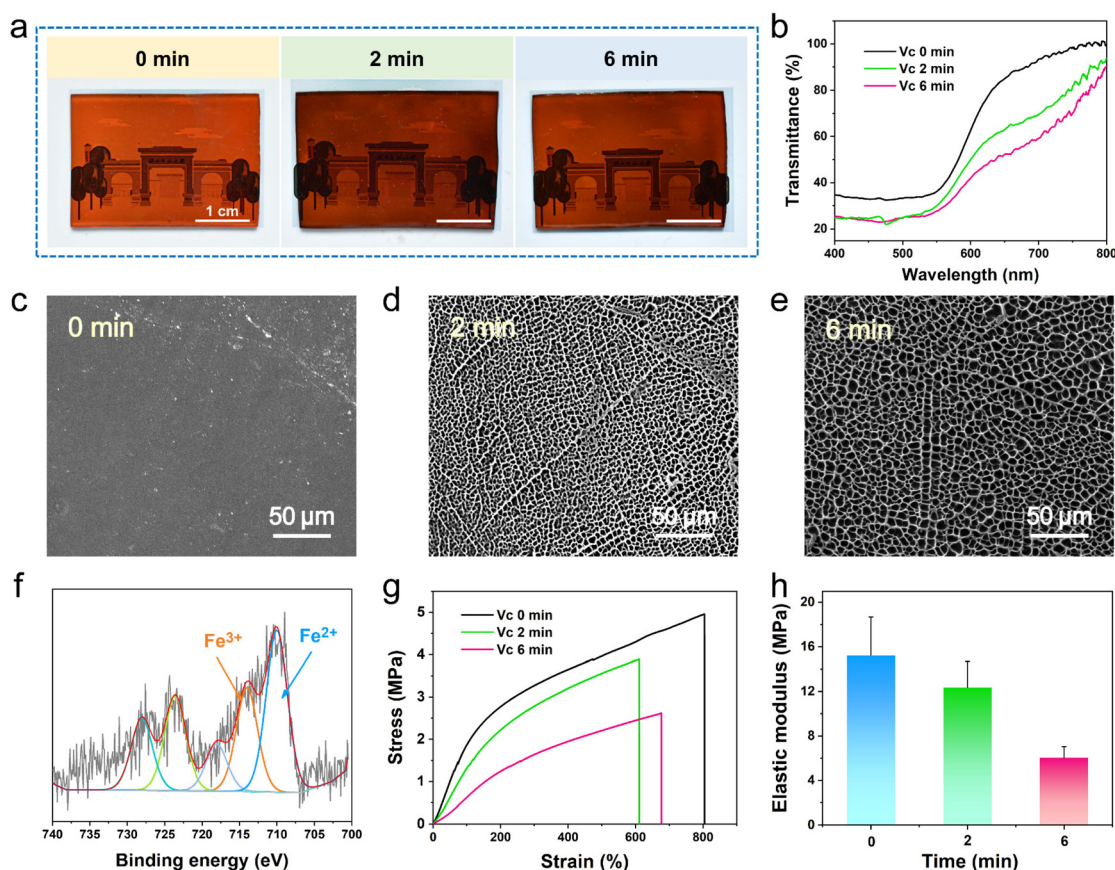

Fig. 2 The characterization of interfacial reduction of Fe^{3+} triggered by Vc (10 mg mL^{-1}). (a) The optical images of the PAM-PAA/Fe^{3+} hydrogel substrate after reduction for 0 min, 2 min and 6 min. (b) The transmittance curves of PAM-PAA/Fe^{3+} hydrogel substrates after reduction for 0 min, 2 min and 6 min. (c–e) The SEM images of PAM-PAA/Fe^{3+} hydrogel substrates after reduction for 0 min, 2 min and 6 min. (f) Fe 2p XPS spectrum of PAM-PAA/Fe^{3+} hydrogel substrates after reduction for 6 min. (g and h) The stress–strain curves and the corresponding elastic moduli of the PAM-PAA/Fe^{3+} hydrogel substrates after reduction for 0 min, 2 min and 6 min.

surface porous structure was observed for the hydrogel after reduction for 2 min and 6 min (Fig. 2d and e). Upon extending the reduction time, the size of pores gradually increases, indicating the dissociation of the Fe^{3+}–COO^- network, arising from the reduction of Fe^{3+} to Fe^{2+}.[43] This fact also supports the above speculation that the surface porous structure allows more light to be reflected and scattered, thereby reducing the light transmittance. Moreover, the longer reduction time will lead to a darker color and larger pore size, because increased Fe^{3+} was reduced to Fe^{2+} upon extending the Vc reduction time. In addition, the reduction of Fe^{3+} to Fe^{2+} was confirmed using an X-ray photoelectron spectrometer (XPS). As shown in Fig. 2f, multiple Fe signals appeared from about 700 eV to 735 eV, and obvious Fe 2p peaks respectively appeared at 710.8 and 713.5 eV, indicating that part of the Fe^{3+} of the hydrogel substrate surface was reduced to Fe^{2+} by Vc.[44] The formation of the surface porous structure has an important impact on the mechanical properties of the hydrogel. Therefore, we evaluated the mechanical properties of the hydrogels with different reduction times (Fig. 2g and h). The tensile strength of the

original hydrogel is ~5 MPa. After reduction with Vc for 2 min and 6 min, the tensile strength decreases to ~4 and 2.5 MPa, respectively, due to the formation of the top porous structure. Similarly, the corresponding elastic modulus decreases from ~15 to 12 and 6 MPa. The longer reduction time endows the hydrogel substrate with weak mechanical properties. Therefore, in order to ensure the mechanical properties of the layered hydrogel, generally, a reduction time of 2 min was selected as an optimal condition. The adjustable amount of produced Fe^{2+} controlled by the Vc reduction time can be further utilized to realize the controllable thickness of the grown hydrogel layer.

Subsequently, the polymerization kinetics of Vc-triggered interfacial self-growth was systematically investigated. The PAM-PAA hydrogel was taken as an example to investigate the effect of the reduction time and concentration of Vc on the thickness of the grown hydrogel layer. As shown in Fig. 3a, the thickness of the PAM-PAA hydrogel layer increases correspondingly from 266 μm to 403 μm upon extending the Vc reduction time from 1 min to 6 min. Fig. 3b shows that the thickness
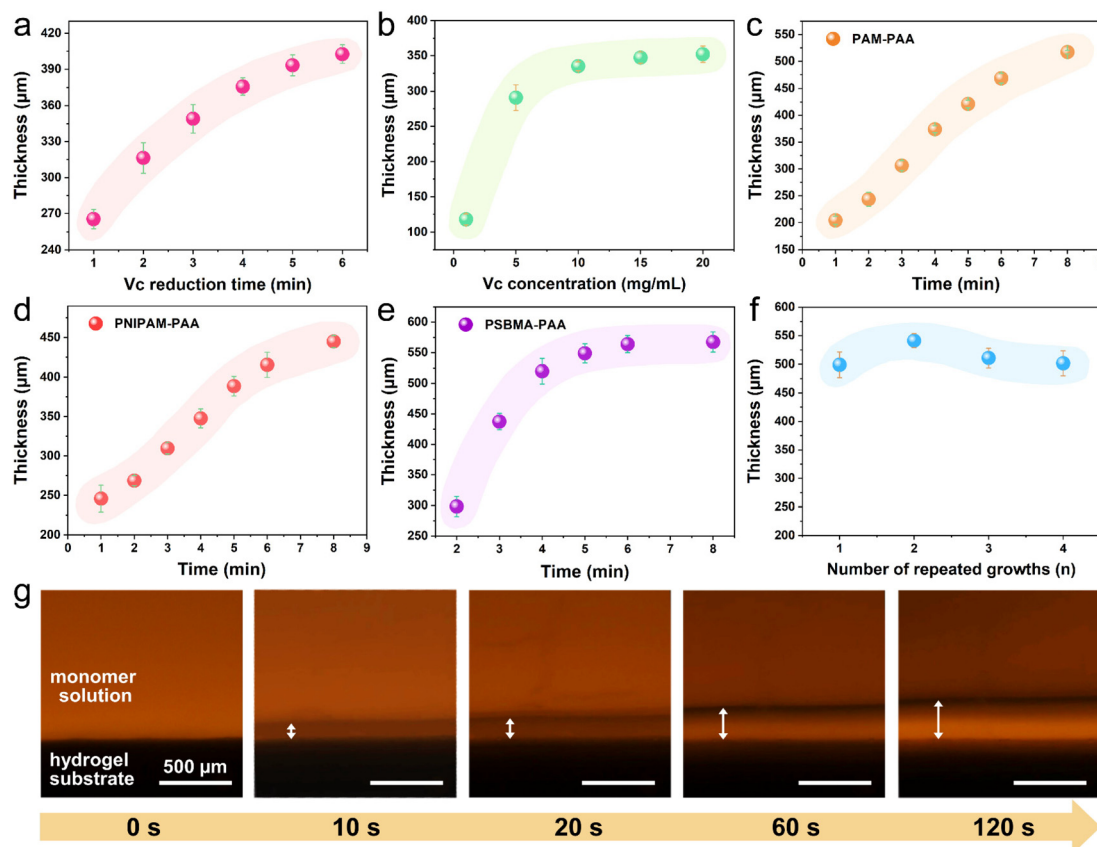
Fig. 3 The polymerization kinetics of Vc-triggered interfacial self-growth. (a) The thickness variation of the self-growing PAM-PAA hydrogel layer with different Vc reduction times (growth time: 3 min, Vc concentration: 10 mg mL^{-1}); (b) the thickness variation of the PAM-PAA hydrogel layer with different Vc concentrations (reduction time: 3 min, growth time: 3 min); (c) the thickness *versus* growth time of the PAM-PAA hydrogel layer (Vc concentration: 10 mg mL^{-1}, reduction time: 2 min); (d and e) the thickness variations of self-growing PNIPAM-PAA and PSBMA-PAA hydrogel layers with different growth times (Vc concentration: 10 mg mL^{-1}, Vc reduction time: 2 min); (f) the reusability of the PAM-PAA/Fe^{3+} hydrogel substrate (Vc reduction time: 2 min, growth time: 4 min); and (g) real-time monitoring of the growth of the PAM-PAA hydrogel layer on the PAM-PAA/Fe^{3+} hydrogel substrate (Vc concentration: 10 mg mL^{-1}, reduction time: 2 min).

also increases from 118 μm to 352 μm with the increase of Vc concentration from 1 mg mL^{-1} to 20 mg mL^{-1}. This is because a longer Vc reduction time and larger Vc concentration will generate more Fe^{2+} catalysts to accelerate the interfacial polymerization rate and thus increase the growth thickness. In addition, the thickness of the grown hydrogel layer is highly dependent on the growth time in the monomer solution (Fig. 3c and S2†). The thickness can reach 517 μm in a growth time of 8 min, indicating the ultrafast and controllable growth of the layered hydrogel. It is obvious that the thickness increases rapidly first and then reaches a plateau upon extending the Vc reduction time and concentration, as well as the growth time. It is worth noting that the grown hydrogel layer limits the diffusion of free radicals during the polymerization process, and thus the growth rate of the hydrogel layer decreases.[45] The compositions of the prepared hydrogel materials were confirmed using Fourier transform infrared spectroscopy (FTIR) (Fig. S3†). Compared with the PAM-PAA/Fe^{3+} hydrogel substrate, the peak of carbonyl (–COOH) groups shifts from 1577 cm^{-1} to 1609 cm^{-1} for the PAM-PAA/Fe^{3+}&PAM-PAA layered hydrogel due to the absence of –COO$^-$–Fe^{3+} coordination. Multiple hydrogels including zwitterionic poly(sulfobetaine methacrylate-acrylic acid) (PSBMA-PAA) and temperature-responsive poly(N-isopropylacrylamide-acrylic acid) (PNIPAM-PAA) hydrogel layers can also be successfully grown, highlighting the universality and robustness of the demonstrated Vc-triggered interfacial self-growing strategy (Fig. 3d and e). It can be seen that the thicknesses of both PSBMA-PAA and PNIPAM-PAA hydrogel layers also exhibit a positive correlation with the growth time. The FT-IR spectra in Fig. S4† also further confirm the successful preparation of layered hydrogels. Surprisingly, the PAM-PAA/Fe^{3+} stiff hydrogel substrate could be reused four times after peeling off the grown hydrogel layer. The thickness of the grown PSBMA-PAA hydrogel layer for four repeated cycles remains around 500 μm (Fig. 3f), which is comparable with the fresh substrate. The repeated use of the stiff hydrogel substrate strongly supports the fact of interfacial radical polymerization, in which the majority of the generated Fe^{2+} catalyst was confined in the hydrogel substrate and the polymerization of the monomer solution was avoided. Moreover, the dynamic growth process of the PAM-PAA hydrogel layer was monitored in real time with the assistance of an optical microscope. The snapshots in Fig. 3g vividly show the formation of a freshly grown hydrogel
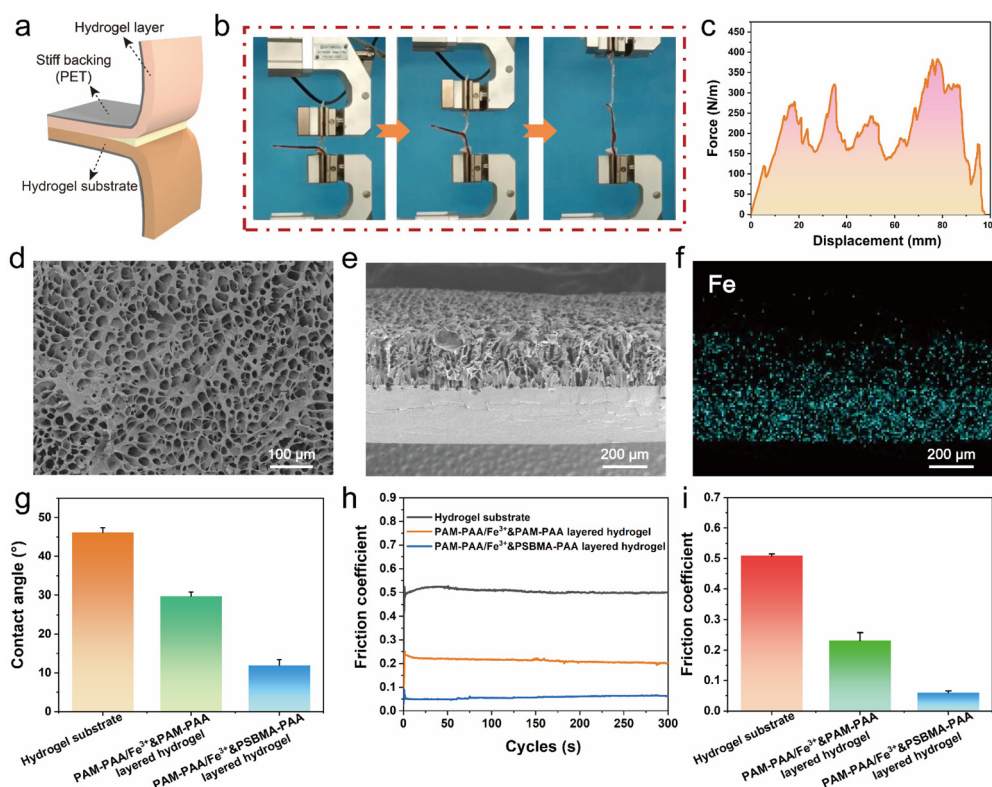

Fig. 4 The characterization of the prepared layered hydrogels. (a) Schematic representation of the 180° peel test for measuring the interfacial bonding force of the layered hydrogel. (b) Snapshots of the 180° peel test. (c) The 180° peeling force *versus* displacement curve of the freshly grown PAM-PAA hydrogel layer and the PAM-PAA/Fe^{3+} stiff hydrogel substrate. (d and e) The superficial and cross-sectional morphology of the PAM-PAA/Fe^{3+}&PAM-PAA layered hydrogel (Vc reduction time: 1 min, growth time: 3 min). (f) The Fe elemental mapping corresponding to (e). (g) The static water contact angle of the PAM-PAA/Fe^{3+} hydrogel substrate, and PAM-PAA/Fe^3&PAM-PAA and PAM-PAA/Fe^3&PSBMA-PAA layered hydrogels. (h and i) The friction curves and mean friction coefficients of the PAM-PAA/Fe^{3+} hydrogel substrate, and PAM-PAA/Fe^3&PAM-PAA and PAM-PAA/Fe^3&PSBMA-PAA layered hydrogels.

layer and the thickness rapidly increases as the time extends to 120 s. The above results of interfacial polymerization kinetics indicate that the demonstrated strategy allows for the rapid and effective preparation of diverse layered hydrogels with controllable thickness, paving the way for the applications of layered hydrogels as actuators.

Furthermore, the interfacial bonding force between the PAM-PAA/Fe^{3+} hydrogel substrate and the grown PAM-PAA hydrogel layer was quantitatively measured by a 180° peel test with polyethylene terephthalate (PET) as a hard backing to prevent hydrogel layer deformation (Fig. 4a). The typical snapshots in Fig. 4b obtained from the peel test perfectly show the peeling process. As is shown in Fig. 4c, the bonding force between the substrate layer and the grown layer can reach about 250 N m^{-1}. Such a high interfacial bonding force can be ascribed to the formed interpenetrated network at the inter-

face. Subsequently, the superficial and cross-sectional morphology and energy dispersive spectroscopy (EDS) mapping further validate the good interfacial bonding force between the PAM-PAA/Fe^{3+} hydrogel substrate and the grown hydrogel layer. As shown in Fig. 4d, the surface of the PAM-PAA/Fe^{3+}&PAM-PAA layered hydrogel exhibits an obvious porous network structure. The layered hydrogel shows an apparent layered structure consisting of the PAM-PAA/Fe^{3+} hydrogel substrate layer with a compact network and the grown PAM-PAA hydrogel layer with a loose and porous network. The two layers are seamlessly combined together to form an interpenetrated network (Fig. 4e). The mapping of the Fe element in Fig. 4f shows that the Fe element is mainly uniformly distributed in the substrate layer, confirming the obvious layered structure. After growing a fresh hydrogel layer, the surface physico-chemical properties (*e.g.* wettability and lubrication) of the
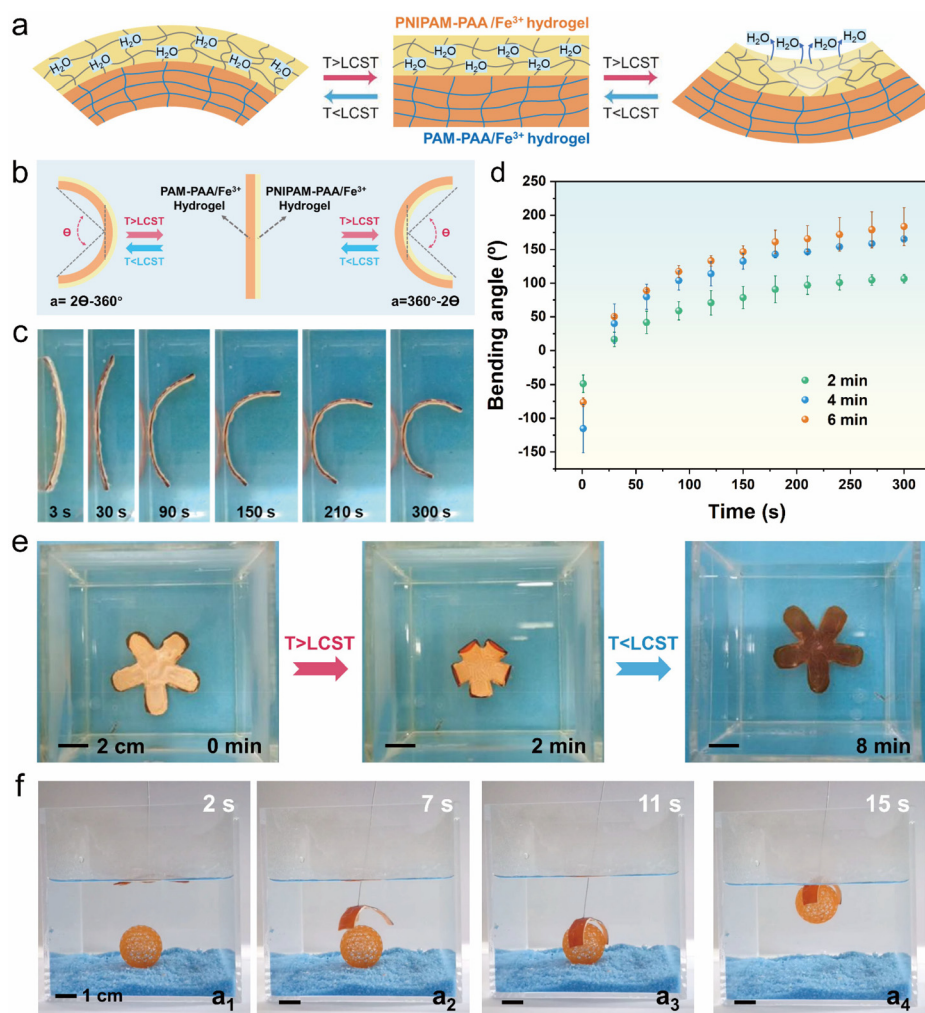
Fig. 5 The actuation behaviors of thermo-responsive layered hydrogels. (a) The schematic diagram of the actuation mechanism of thermo-responsive PAM-PAA/Fe^{3+}&PNIPAM-PAA/Fe^{3+} layered hydrogels. (b) Schematic diagram of bending angle measurement of strip-like layered hydrogels. (c) The snapshots of the bending process of strip-like layered hydrogels (growth time: 6 min). (d) The corresponding bending angle *versus* growth time of strip-like layered hydrogels. (e) The real-time image of the actuating behavior of the five-petal flower-like layered hydrogel actuator underwater in response to different temperatures. (f) A demonstration of the three-clawed layered hydrogel manipulator capturing objects from warm water (~60 °C).

hydrogel substrate will change. Specifically, the water static contact angle of the PAM-PAA/Fe^{3+} substrate is 46°, while it reduces to 30° and 12° after growing PAM-PAA and PSBMA-PAA hydrogel layers (Fig. 4g). Correspondingly, the coefficient of friction reduces from 0.51 to 0.23 and 0.06, respectively (Fig. 4h and i). The decrease of the contact angle and coefficient of friction is attributed to the highly hydrophilic feature as well as the loose network of the grown hydrogel layer compared with the PAM-PAA/Fe^{3+} stiff hydrogel substrate.

Designing a patterned layered hydrogel with controllable shape and size was vital for extending applications. The demonstrated method allows for the preparation of a patterned layered hydrogel with the assistance of the pen direct writing strategy.[46] Typically, the Vc solution was employed as ink for writing patterns to selectively reduce localized Fe^{3+}, resulting in the growth of the patterned layered hydrogel in the reduced regions. As shown in Fig. S5,† various patterned layered hydrogels like letters "ABC" and numbers "123" (left) can be successfully prepared and become fluorescent after dyeing with rhodamine B (right), implying its potential for achieving complicated structural designs for layered hydrogels. Besides, the thermo-responsive PAM-PAA/Fe^{3+}&PNIPAM-PAA/Fe^{3+} layered hydrogel can be successfully prepared after growing the temperature-responsive PNIPAM-PAA hydrogel and subsequently immersing it in $FeCl_3 \cdot 6H_2O$ solution for ionic coordination to strengthen the grown PNIPAM-PAA hydrogel network. The thermal-response mechanism of the PAM-PAA/Fe^{3+}&PNIPAM-PAA/Fe^{3+} layered hydrogel is demonstrated in Fig. 5a. When the temperature of the water bath is higher than the low critical solution temperature (LCST) of PNIPAM, the PNIPAM polymer chains will dehydrate and result in contraction and modulus increment of the PNIPAM-PAA/Fe^{3+} hydrogel layer, while the PAM-PAA/Fe^{3+} hydrogel substrate layer remains unchanged. Such a dehydration-induced stress difference will lead to curving toward the grown layer direction. Inversely, when the temperature of the water bath is lower than the LCST, the PNIPAM polymer chains will rehydrate, followed by swelling and a decrease of the modulus of the PNIPAM-PAA/Fe^{3+} hydrogel layer, resulting in bending toward the substrate layer. Fig. 5b shows the thermo-responsive bending and recovery process of long strip-like PAM-PAA/Fe^{3+}&PNIPAM-PAA/Fe^{3+} layered hydrogels and the method for measuring the bending angle in detail. As shown in Fig. 5c, the bending angle of the layered hydrogel increases with the increase of the response time and then remains constant upon immersing it in a 60 °C water bath for 300 s. At the beginning, at room temperature (<LCST), it will bend toward the stiff substrate layer, so the bending angle is negative. After immersing it in the 60 °C water bath, it will first change to a straight state and then curve toward the grown responsive layer to result in a positive bending angle. The growth time of the responsive PNIPAM-PAA/Fe^{3+} hydrogel layer also has an effect on the bending angle due to the different thicknesses. The bending angle continuously increases with the increase of the growth time from 2 min to 6 min (Fig. 5d), which is attributed

to the thickness increment of the PNIPAM-PAA/Fe^{3+} hydrogel layer to produce a larger driving force. Typically, when the growth time is 6 min, the bending angle remains as high as 184° upon immersing it in the 60 °C water bath. Moreover, a bilayered hydrogel actuator with a five-petal flower-like structure is created by cutting the prepared layered hydrogel sheet and its complex shape deformation in water baths with different temperatures can also be achieved. Upon immersing the five-petal flower-like layered hydrogel actuator in a 60 °C water bath, the actuator bends towards the PNIPAM-PAA/Fe^{3+} hydrogel side, and it will recover to the original state after putting it in a 25 °C water bath (Fig. 5e). More interestingly, the potential application of the layered hydrogel actuator as a smart underwater manipulator was demonstrated. A three-claw layered hydrogel actuator was constructed. It was able to successfully capture objects like small balls and plastic fish from warm water due to the mechanical deformation force (Fig. 5f and S6†). Above all, the prepared layered hydrogel actuators will have potential applications in the field of intelligent soft robots.

Conclusion

In summary, we proposed a facile self-growing method for constructing robust layered hydrogel actuators by crafting Vc-triggered interfacial radical polymerization from a stiff hydrogel. Using the demonstrated strategy, various layered hydrogels can be fabricated rapidly and the thickness of the grown hydrogel layer can be accurately regulated by changing the growth time, Vc reduction time and Vc concentration. The obtained layered hydrogel actuator exhibits two asymmetric structural layers, a dense and stiff layer and a porous and loose layer, as well as a strong interfacial bonding force of about 250 N m^{-1} between the porous layer and the stiff substrate. Furthermore, a thermo-responsive layered hydrogel actuator was developed, which displayed reversible underwater bending behavior in response to temperature changes. The excellent actuation performance is ascribed to the dehydration-induced shrinkage stress of the grown responsive hydrogel layer in combination with the strong interfacial bonding force. Interestingly, a smart manipulator based on the thermo-responsive layered hydrogel actuator was demonstrated to capture objects underwater. Overall, our method provides a novel and feasible approach for highly efficient and controllable preparation of layered hydrogel actuators, which will find promising applications in the fields of soft robotics, intelligent devices, sensors and so on.

Data availability

As the corresponding author of this paper, I, Qiangbing Wei, hereby on behalf of all authors declare that the main data supporting the findings of this article are available within the manuscript and its ESI.†

Conflicts of interest

There are no conflicts to declare.

Acknowledgements

References

1 Y. Forterre, J. M. Skotheim, J. Dumais and L. Mahadevan, *Nature*, 2005, **433**, 421–425.

2 P. Fratzl and F. G. Barth, *Nature*, 2009, **462**, 442–448.

3 A. G. Volkov, J. C. Foster, T. A. Ashby, R. K. Walker, J. A. Johnson and V. S. Markin, *Plant, Cell Environ.*, 2010, **33**, 163–173.

4 B. Wu, H. Lu, X. Le, W. Lu, J. Zhang, P. Théato and T. Chen, *Chem. Sci.*, 2021, **12**, 6472–6487.

5 D. Jiao, Q. L. Zhu, C. Y. Li, Q. Zheng and Z. L. Wu, *Acc. Chem. Res.*, 2022, **55**, 1533–1545.

6 W. Li, Q. Guan, M. Li, E. Saiz and X. Hou, *Prog. Polym. Sci.*, 2023, **140**, 101665.

7 J. Shang, X. Le, J. Zhang, T. Chen and P. Theato, *Polym. Chem.*, 2019, **10**, 1036–1055.

8 M. Baumgartner, F. Hartmann, M. Drack, D. Preninger, D. Wirthl, R. Gerstmayr, L. Lehner, G. Mao, R. Pruckner and S. Demchyshyn, *Nat. Mater.*, 2020, **19**, 1102–1109.

9 Y. Cheng, K. H. Chan, X.-Q. Wang, T. Ding, T. Li, X. Lu and G. W. Ho, *ACS Nano*, 2019, **13**, 13176–13184.

10 M.-K. Shin, G. M. Spinks, S. R. Shin, S. I. Kim and S. J. Kim, *Adv. Mater.*, 2009, **21**, 1712–1715.

11 M. Chen, G. Song, B. Ren, L. Cai, M. Hossain and C. Chang, *Chem. Eng. J.*, 2023, **475**, 146047.

12 Y. Ma, Y. Zhang, B. Wu, W. Sun, Z. Li and J. Sun, *Angew. Chem., Int. Ed.*, 2011, **50**, 6254–6257.

13 D. Morales, E. Palleau, M. D. Dickey and O. D. Velev, *Soft Matter*, 2014, **10**, 1337–1348.

14 Q. L. Zhu, C. Du, Y. Dai, M. Daab, M. Matejdes, J. Breu, W. Hong, Q. Zheng and Z. L. Wu, *Nat. Commun.*, 2020, **11**, 5166.

15 Z. Lu, L. Sun, J. Liu, H. Wei, P. Zhang and Y. Yu, *ACS Macro Lett.*, 2022, **11**, 967–974.

16 J. Zhang, K. Yan, J. Huang, X. Sun, J. Li, Y. Cheng, Y. Sun, Y. Shi and L. Pan, *Adv. Funct. Mater.*, 2024, **34**, 2314433.

17 Q. Xu, M. Hou, L. Wang, X. Zhang and L. Liu, *Chem. Eng. J.*, 2023, **477**, 147065.

18 J. Zhao and J. Bae, *Adv. Funct. Mater.*, 2022, **32**, 2200157.

19 W. C. Huang, R. Ying, W. Wang, Y. Guo, Y. He, X. Mo, C. Xue and X. Mao, *Adv. Funct. Mater.*, 2020, **30**, 2000644.

20 E. Wang, M. S. Desai and S.-W. Lee, *Nano Lett.*, 2013, **13**, 2826–2830.

21 P. Xue, H. K. Bisoyi, Y. Chen, H. Zeng, J. Yang, X. Yang, P. Lv, X. Zhang, A. Priimagi and L. Wang, *Angew. Chem., Int. Ed.*, 2021, **60**, 3390–3396.

22 X. He, D. Zhang, J. Wu, Y. Wang, F. Chen, P. Fan, M. Zhong, S. Xiao and J. Yang, *ACS Appl. Mater. Interfaces*, 2019, **11**, 25417–25426.

23 J. H. Park, S. W. Lee, D. S. Song and J. Y. Jho, *ACS Appl. Mater. Interfaces*, 2015, **7**, 16659–16667.

24 X. Le, W. Lu, J. Zhang and T. Chen, *Adv. Sci.*, 2019, **6**, 1801584.

25 C. Yao, Z. Liu, C. Yang, W. Wang, X.-J. Ju, R. Xie and L.-Y. Chu, *Adv. Funct. Mater.*, 2015, **25**, 2980–2991.

26 C. Ma, W. Lu, X. Yang, J. He, X. Le, L. Wang, J. Zhang, M. J. Serpe, Y. Huang and T. Chen, *Adv. Funct. Mater.*, 2018, **28**, 1704568.

27 Y. Xiang, C. Liu, S. Ma, X. Wang, L. Zhu and C. Bao, *Adv. Funct. Mater.*, 2023, **33**, 2300416.

28 M. S. Oh, Y. S. Song, C. Kim, J. Kim, J. B. You, T.-S. Kim, C.-S. Lee and S. G. Im, *ACS Appl. Mater. Interfaces*, 2016, **8**, 8782–8788.

29 Z. Li, Y. Su, B. Xie, H. Wang, T. Wen, C. He, H. Shen, D. Wu and D. Wang, *J. Mater. Chem. B*, 2013, **1**, 1755–1764.

30 K. D. Seo, J. Doh and D. S. Kim, *Langmuir*, 2013, **29**, 15137–15141.

31 X. Zhang, M. Jin, L. Ding, J. He, Y. Bai and L. Zhang, *Chem. Eng. J.*, 2023, **468**, 143734.

32 H. Lu, B. Wu, X. Yang, J. Zhang, Y. Jian, H. Yan, D. Zhang, Q. Xue and T. Chen, *Small*, 2020, **16**, 2005461.

33 R. Zhang, P. Lin, W. Yang, M. Cai, B. Yu and F. Zhou, *Polym. Chem.*, 2017, **8**, 7102–7107.

34 L. Ionov, *Mater. Today*, 2014, **17**, 494–503.

35 H. Wang, X. Xiong, H. Luo, Y. Cui, Q. Wu, Y. Fang, J. Chen, G. Jing and J. Cui, *Angew. Chem., Int. Ed.*, 2024, e202407125.

36 X. Xiong, H. Wang, L. Xue and J. Cui, *Angew. Chem., Int. Ed.*, 2023, **62**, e202306565.

37 Y. Fang, Q. Chang, X. Xiong, S. Dong, C. Zhang, L. Yang and J. Cui, *Adv. Funct. Mater.*, 2022, **32**, 2206222.

38 R. Xu, M. Hua, S. Wu, S. Ma, Y. Zhang, L. Zhang, B. Yu, M. Cai, X. He and F. Zhou, *Matter*, 2022, **5**, 634–653.

39 R. Xu, Y. Zhang, S. Ma, Z. Ma, B. Yu, M. Cai and F. Zhou, *Adv. Mater.*, 2022, **34**, 2108889.

40 H. Quan, A. Pirosa, W. Yang, R. O. Ritchie and M. A. Meyers, *Acta Biomater.*, 2021, **128**, 370–383.

41 K. Song, E. Yeom, S.-J. Seo, K. Kim, H. Kim, J.-H. Lim and S. J. Lee, *Sci. Rep.*, 2015, **5**, 9963.

42 J. Bolobajev, M. Trapido and A. Goi, *Chem. Eng. J.*, 2015, **281**, 566–574.

43 R. Zhang, Y. Zhang, Y. Li, X. Hu, J. Zhen and Z. Jia, *Tribol. Int.*, 2023, **184**, 108436.

44 J. Wang, T. Li, F. Chen, D. Zhou, B. Li, X. Zhou, T. Gan, S. Handschuh-Wang and X. Zhou, *Macromol. Rapid Commun.*, 2018, **39**, e1800143.

45 B. Wu, H. Lu, Y. Jian, D. Zhang, Y. Peng, J. Zhuo, X. Le, J. Zhang, P. Théato and T. Chen, *CCS Chem.*, 2023, **5**, 704–717.

46 S. W. Song, S. Lee, J. K. Choe, N.-H. Kim, J. Kang, A. C. Lee, Y. Choi, A. Choi, Y. Jeong and W. Lee, *Sci. Adv.*, 2021, **7**, eabf3804.